RBS-channeling study of radiation damage in Ar^+ implanted $CuInSe_2$ crystals

Michael V. Yakushev[a)]
Department of Physics, SUPA, Strathclyde University, Glasgow G4 0NG, United Kingdom; Ural Federal University, Ekaterinburg 620002, Russia; and Institute of Solid State Chemistry of the Urals Branch of RAS, Ekaterinburg 620990, Russia

Vladimir A. Volkov
Ural Federal University, Ekaterinburg 620002, Russia

Niyazi N. Mursakulov and Chimnaz E. Sabzaliyeva
Institute of Physics, National Academy of Sciences of Azerbaijan, H.Cavid ave., 33, AZ-1143 Baku, Azerbaijan

Robert W. Martin
Department of Physics, SUPA, Strathclyde University, Glasgow G4 0NG, United Kingdom

(Received 4 June 2016; accepted 17 August 2016; published 26 August 2016)

Chalcopyrite solar cells are reported to have a high tolerance to irradiation by high energy electrons or ions, but the origin of this is not well understood. This work studies the evolution of damage in Ar^+-bombarded $CuInSe_2$ single crystal using Rutherford backscattering/channeling analysis. Ar^+ ions of 30 keV were implanted with doses in the range from 10^{12} to 3×10^{16} cm^{-2} at room temperature. Implantation was found to create two layers of damage: (1) on the surface, caused by preferential sputtering of Se and Cu atoms; (2) at the layer of implanted Ar, possibly consisting of stacking faults and dislocation loops. The damage in the second layer was estimated to be less than 2% of the theoretical prediction suggesting efficient healing of primary implantation defects. © *2016 American Vacuum Society*. [http://dx.doi.org/10.1116/1.4961882]

I. INTRODUCTION

The ternary compound $CuInSe_2$ is a semiconductor with the chalcopyrite structure.[1] This material is used in the absorber layers of solar cells with the current record values for conversion efficiency for photovoltaic devices (21.8% for laboratory size thin-film cells[2]). The $CuInSe_2$—based solar cells are also known for their exceptional tolerance to high energy electron and ion radiation.[3–5] Ions of noble gases are convenient particles to study physical mechanisms of radiation damage generated by ion implantation because they do not form chemical bonds.

Rutherford backscattering (RBS) is an experimental technique which can provide reliable information on the elemental composition.[6] Combining RBS with the ion channeling effect (RBS/C) by aligning the beam of high energy positive ions with low index axes of the lattice provides information on the near surface depth profile of the concentration of structural defects in the lattice. Such an alignment dramatically reduces the backscattered yield which then becomes very sensitive to the presence of structural defects and, in particular, to interstitial atoms blocking the channels, space between the strings of positively charged nuclei along low index axes in the host lattice, and causing excessive backscattering yield. These significantly increase the channeled backscattering yield allowing the RBS/C spectra to provide rich quantitative information on the type of atoms blocking the channels, their concentration, and concentration depth profile.[6] The higher the structural quality of the host lattice the greater the amount of information that can be gained from the RBS/C yield from the defects. However, it is difficult to grow $CuInSe_2$ crystals with high structural quality because of the complicated phase diagram[7] and not many reports demonstrate the application of RBS/C for analysis of structural defects in $CuInSe_2$.[8–10]

In this study, we report on the use of the RBS/C technique to study depth resolved concentrations of defects, generated by different doses of a 30 keV argon ion beam, separately in the copper, indium, and selenium sublattices of high structural quality $CuInSe_2$ single crystals.

II. EXPERIMENT

A *p*-type conductivity $CuInSe_2$ single crystal with dimensions 2×1 cm and thickness of 2 mm was cut from the middle part of an ingot grown by the vertical Bridgman technique, from a near stoichiometric charge.[11] The sample was mechanically polished with different grade diamond pastes and finished in a vibrating bath with 0.05 μm alumina slurry. The polished sample was etched in a 0.1% Br in methanol solution for 1 min, and then annealed in vacuum at 300 °C to remove the selenium layer left at the surface due to the etch.[12] The orientation of the crystal was established using x-ray Laue patterns prior to implantation. The surface of the sample was found to be within 5° of the (112) plane. After the surface preparation, the sample was implanted at room temperature with 30 keV Ar^+ with doses from 10^{12} to 3×10^{16} cm^{-2} at ion current density 3 $\mu A/cm^2$.

In order to avoid unintentional channeling during implantation, the argon ion beam was set up about 3° away the ⟨221⟩ axis used for RBS/C analysis. Different doses were

a)Electronic mail: michael.yakushev@strath.ac.uk

implanted into stripes of 3 mm width. One area was left unimplanted to serve as a reference.

RBS/C measurements were carried out using 2 MeV He^+ ions in the normal incidence beam geometry and with a 168° backscattering angle. The energy resolution of this type of analysis is normally close to $\delta = 25$ keV which is equivalent to five channels in the RBS spectra or to 35 nm in depth terms for near-surface layers. Before each measurement, the absolute position of the RBS spectra was calibrated, so the absolute accuracy was close to 1–2 channels (equivalent to 7.5–15 nm in terms of depth). The homogeneity of the lattice was established by taking aligned spectra at various points across the surface prior to implantation. The aligned spectra were collected with the beam directed along the ⟨221⟩ axis. The random spectra were collected directing the ion beam 5° away from the ⟨221⟩ axis while slowly tilting the samples about this axis to avoid channeling effects from axes and planes. The random and aligned spectra in the crystal before implantation are shown in Fig. 1. The dechanneling parameter $\chi_{\min} = Y_{a\mathrm{Inmin}}/Y_{r\mathrm{In}}$ (where $Y_{a\mathrm{Inmin}}$ is the minimum backscattering yield in the In related part of the aligned spectra and $Y_{r\mathrm{In}}$ is corresponding backscattering yield in the random spectrum) was found to be $6.2 \pm 0.2\%$, where 0.2% is the statistical error of the mean value. The random and aligned spectra for doses from 1.5×10^{15} to 3×10^{16} cm^{-2} together with one from the virgin area are shown in Fig. 2.

III. CALCULATION PROCEDURE

The RBS spectra from ternary compounds can be considered to be a sum of the three separated RBS yields corresponding to the three atomic species. Each yield is shifted on the energy scale according to the element mass. In our work, we decompose these three yields from the total aligned spectrum of $CuInSe_2$. Channels above channel 328 in the RBS spectra are associated with In. The RBS yield from Se is shifted by about 21 channels to lower energies. Below the 328 channel, it is overlapped with the In yield. The Cu yield is further shifted by 15 channels and is overlapped by both the In and Se yields. Let us first consider the aligned spectrum of the virgin crystal shown in Figs. 1 and 3(a). The three surface peaks in this spectrum are associated with direct backscattering from Cu (the first element in $CuInSe_2$), In (the second element), and Se (the third element) atoms on the surface. The In part of the aligned spectrum before the In surface peak was approximated by a straight regression line $y_2 = x \times k_2 + b_2$ (where x is the channel number whereas k_2 and b_2 are the line parameters) fitted to the experimental points of the linear part of the aligned spectrum between the In and Se surface peaks as shown in Fig. 3(a). Extrapolating the y_2 line, we can use it as the indium background which we can subtract from the total aligned spectrum in order to obtain the selenium yield. The accuracy of the selenium aligned yield includes the statistical error, calculated as the standard deviation of the number of counts assuming a Poisson distribution, as well as the error of the straight regression line y_2 extrapolating the flat part of the spectrum between the In and Se surface peaks. An error of ±12% is estimated for the normalized minimum Se yield. Extrapolating the y_3 line, fitted into the flat part of the aligned spectrum between the selenium and copper surface peaks, we

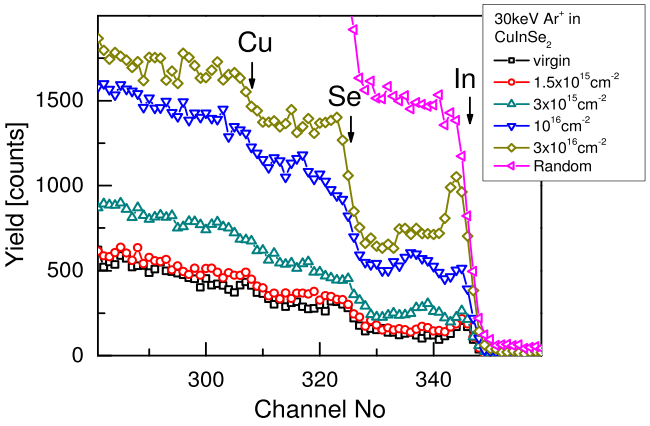

FIG. 2. (Color online) Effect of 30 keV Ar^+ irradiation on the RBS aligned spectra of 2 MeV He^+ from a $CuInSe_2$ crystal.

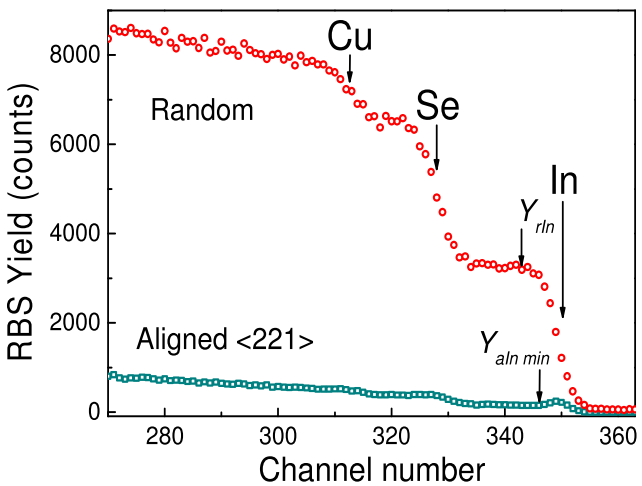

FIG. 1. (Color online) RBS random (○) and aligned (□) (for the ion beam oriented along the ⟨221⟩ direction) spectra in the $CuInSe_2$ single crystal prior to Ar ion implantation.

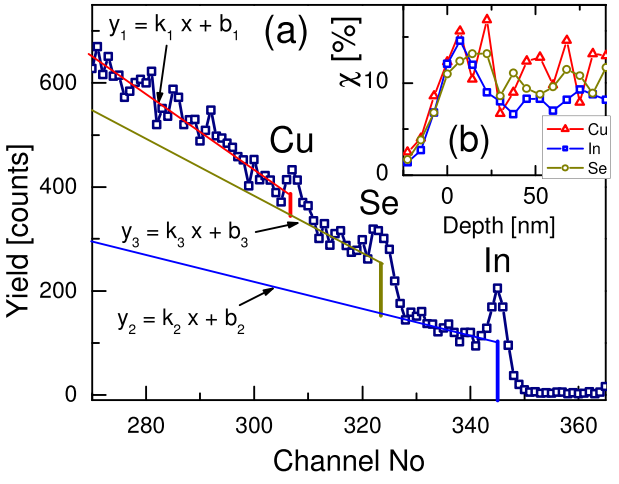

FIG. 3. (Color online) Linear approximation of an aligned spectrum of 2 MeV He^+ channeled along ⟨221⟩ axis measured from the nonimplanted $CuInSe_2$ sample (a); normalized RBS aligned yields $\chi(d)_v$ from Cu, In, and Se after decomposition of the aligned spectrum (b).

can further subtract the selenium background for the copper yield. The accuracy of the normalized copper aligned yield includes errors of the y_3 as well as y_2 lines resulting in an error of $\pm 23\%$. The accuracy of this decomposition procedure depends on the element mass and concentration deteriorating for lighter elements and lower concentrations. Therefore, in this paper, we primarily concentrate on results for the In and Se sublattices.

The random yields corresponding to different elements (Y_{r1}, Y_{r2}, and Y_{r3}) were derived using the same approach. More details on the decomposition procedure can be found in Ref. 13. As a result, three normalized functions $\chi(x)_{vi} = Y_{ai}/Y_{ri}$ for each element (i) were calculated for the virgin area of the crystal. The stopping cross section was calculated using the Bragg's rule assuming the linear additivity of stopping cross sections for Cu, In, and Se in homogeneous $CuInSe_2$. Then, the channel number scale was converted into depth d using the surface energy approximation which ignores changes of the stopping cross section within the depth of analysis (about 100 nm).[6] Differences between the energy losses for channeling and nonchanneling ions were not taken into account. The dependencies of $\chi(d)_{vi}$ on depth for all the three elements are plotted in Fig. 3(b). It can be seen that the values are quite close, although $\chi(d)_{v\mathrm{Cu}}$ has a greater scatter.

Let us consider the aligned spectra of the argon implanted areas shown in Fig. 2. Separated aligned yields Y_a for the three elements from the Ar^+-implanted areas of the sample were obtained and then normalized by Y_r. The dependencies of $\chi(d)_{di}$ on depth for all the three elements for the damaged areas were calculated. The depth available for this analysis depends on differences in the masses of the target elements and on the mass and energy of the ions used for the RBS probe. In the case of $CuInSe_2$ and a 2 MeV He^+ ion beam, such an element sensitive depth resolved analysis can be achieved for depths up to about 100 nm.

The normalized depth profiles $n_i(d)$ of defect concentration for each element were derived from the normalized functions $\chi(d)_{vi}$ and $\chi(d)_{di}$ using the common iterative calculation approach.[14] These profiles show what percentage of the atoms is randomly displaced from their lattice sites, where they block the channels and cause excessive backscattering. Concentrations of copper, indium, and selenium sublattice-related scattering centers were calculated on the assumption of a homogeneous distribution of the ion flux in the transverse plane of the channels. The calculations are performed assuming a multiple scattering mechanism approach with $n_i(d)$ multiplied by an α-parameter, which is adjusted to bring the concentration profile at high depths (tail) of $n_{\mathrm{In}}(d)$ to zero. Such calculations, made without an adjusting parameter, lead to negative values in the tail, whereas the profiles calculated employing the single scattering model do not go to zero with increasing depth. If after the adjustment of $n_{\mathrm{In}}(d)$ the selenium and copper related concentration profile tails also go to zero, we can assume that all the three sublattices have similar types of defects. Otherwise the defect types in different sublattices have different dechanneling cross-sections suggesting different nature of the defects. For a more accurate calculation of the concentration profiles of damage we have to know the dechanneling of the defects in the damaged layer. These cross-sections depend on the defect nature and their locations in the lattice. Without this additional information, the derived values can be used only as a rough first order estimate of the defect depth concentration: namely, the concentration of copper, indium, and selenium atoms randomly displaced from their lattice sites. The absolute accuracy of such estimates can be quite low, for example, in the case of extended defects. Such defects have rather different dechanneling effects compared to arrays of randomly displaced scattering centers. However, this method can give interesting and unique information when used to estimate the amounts of accumulated damage. This method has previously been used earlier to calculate damage concentration depth profiles for the three sublattices in $CuInSe_2$ single crystals following 40 keV Xe^+ implantation[15] and after 2.5 keV H^+ implantation.[9]

IV. RESULTS AND DISCUSSION

Peaks, related to the lattice damage, can be seen in the aligned spectra after implantation of Ar^+ shown in Fig. 2. The above method is employed to derive the concentration depth profiles of scattering centers n_{Cu}, n_{In}, and n_{Se} in the Cu, In, and Se sublattices, respectively. The In and Se profiles are shown in Figs. 4(a) and 4(b), respectively. Similar profiles for the copper sublattice are also determined but showed a high scatter and are not shown. The In-related depth profiles are adjusted to bring their tails to zero using α. The same value of α was then used in the calculations of the selenium and copper depth profiles. However, their tails did not go to zero as shown in Fig. 5(b) for the highest dose of 3×10^{16} cm^{-2}, suggesting differences in the defect nature for each sublattice or/and by deviations in the material stoichiometry caused by the implantation.

It can be seen in Fig. 4 that the concentration profiles of both In and Se consist of two peaks: (P1)—a narrow peak at the surface and (P2)—a wider peak at a depth of 40 nm. In the case of In profiles, which have a lower scatter, the shape

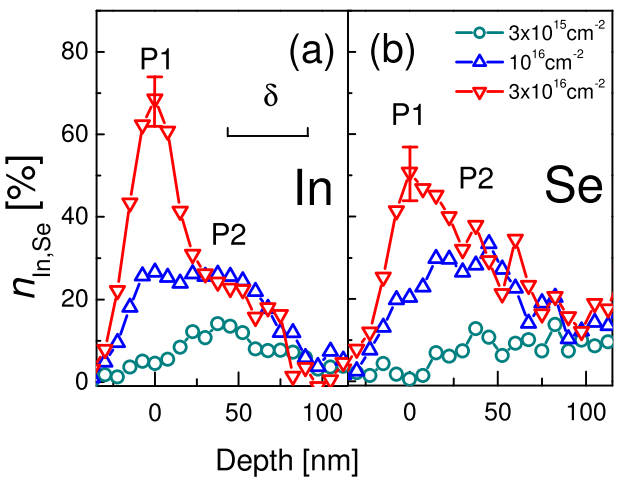

FIG. 4. (Color online) Depth profiles of $n(d)$ concentrations of scattering centers in the (a) In and (b) Se sublattices after 30 keV Ar^+ implantation.

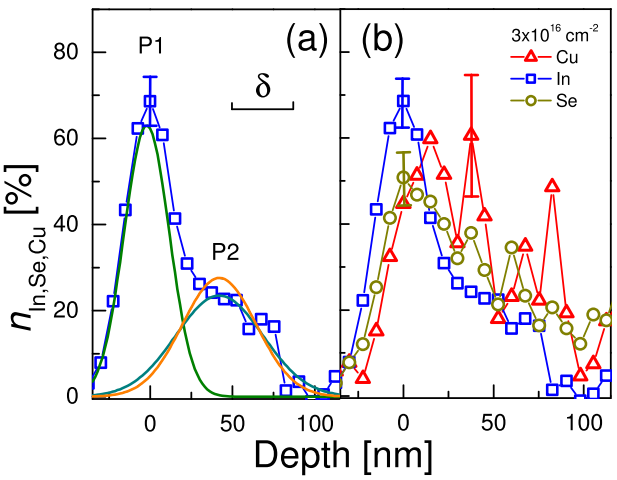

FIG. 5. (Color online) (a) Concentration depth profiles $n(d)$ of the In scattering centers after $3 \times 10^{16}\,\mathrm{cm}^{-2}$ of Ar^+ with fitted Gaussians; (b) concentration depth profiles $n(d)$ of the Cu, In, and Se scattering centers after $3 \times 10^{16}\,\mathrm{cm}^{-2}$ of Ar^+.

of these peaks can be well described by Gaussian curves. An example of Gaussian curve, fitted to the depth profile of In atoms after a dose of $3 \times 10^{16}\,\mathrm{cm}^{-2}$, is shown in Fig. 5(a). The width of this P1 peak is close to the depth-resolution. It implies that its shape has been considerably modified by the lack of resolution. Therefore, we propose to interpret the P1 peak as a result of a thin "amorphous" layer. This layer might retain a certain lattice symmetry, but the He^+ ions do not channel within it. The height of this P1 peak does not reach the random value because of a lack of depth resolution. Evolution of the accumulated damage related to P1, calculated as an area under the P1 peak for each dose, is shown in Fig. 6. It grows almost linearly without signs of saturation.

The second peak (P2) appears in the aligned spectra at a depth of 40 nm after doses above $1.5 \times 10^{15}\,\mathrm{cm}^{-2}$. The peak intensity grows with increasing dose showing saturation at doses over $10^{16}\,\mathrm{cm}^{-2}$. The higher resolution for the indium related RBS yield allows the P1 and P2 peaks to be resolved in the indium depth profiles whereas in the case of selenium these peaks are merged. The P2 peaks for different doses of

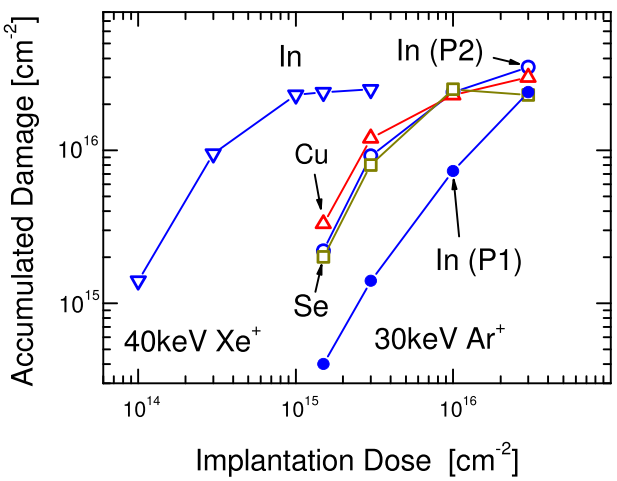

FIG. 6. (Color online) Damage accumulated in Cu, In, and Se sublattices after implantation of $CuInSe_2$ with 40 keV Xe^+ and 30 keV Ar^+.

Ar^+ were successfully fitted with Gaussian curves. Deconvolution of this curve, also shown in Fig. 5(a), results in a slightly reduced estimate of its full width at half maximum (FWHM) $W_{P2} = 45$ nm. The evolution of the accumulated damage related to P2, calculated as an area under the P2 peak for each dose and element, is shown in Fig. 6. The accumulated damage clearly saturates at doses over 3×10^{15} cm^{-2} for all the three elements.

The P1-peak can be attributed to the effect of preferential sputtering. A selenium deficient layer was detected after 5 keV Ar^+-sputtering of $CuInSe_2$ single crystals using Auger electron spectroscopy.[16] An x-ray photoelectron spectroscopy study[17] of $CuInSe_2$ single crystals sputtered using 0.5 keV Ar^+ revealed the presence of an indium layer with a copper deficient surface of $CuInSe_2$ (the ordered vacancy compound $CuIn_3Se_5$ and the binary phase In_2Se_3) under this layer.

The $n(d)$ depth profiles for the indium, selenium, and copper sublattices after implantation of 3×10^{16} cm^{-2} of Ar^+, shown in Fig. 5(b), all suggest a similar picture. The indium peak P1 in this diagram is consistent with a thin indium layer on the surface. TRIM-code[18] (a Monte-Carlo programme simulating ion interaction with matter) calculations of the mean numbers of atoms sputtered from $CuInSe_2$ by one 30 keV Ar^+ ion (Cu–1.93; In–1.71; Se–4.01) also confirmed preferential sputtering of Se and Cu. Preferential sputtering can explain why additional adjustment coefficients α have to be used for depth profile calculations.

The P2-peak is attributed to the effect of radiation damage created by Ar^+ ions at the end of the collision cascades. The concentration depth profiles of 30 keV Ar^+ in $CuInSe_2$ and radiation-induced vacancy distributions were calculated using the TRIM-code. The mean penetration depth for Ar^+ and the FWHM of the depth profile are found to be $R_{Ar} = 27$ nm and $W_{Ar} = 30$ nm, respectively. Radiation-induced vacancy depth profiles are calculated to be slightly shallower, with a maximum at about $R_{Vac} = 16$ nm and a FWHM $W_{Vac} = 42$ nm. The depth of the defect maximum is significantly smaller than the experiment value $R_{P2} = 40$ nm.

To explain the results, we propose a physical model. This model is based on the assumption of a high mobility of point defects in $CuInSe_2$ at room temperature. This assumption is supported by theoretical calculations of the defect formation energies in $CuInSe_2$ (Ref. 19) and experimental evidence of significant mobility of copper interstitial atoms.[20,21] The mobility of copper interstitial can be enhanced by thermal spikes, generated by energetic Ar ions. Theoretical estimates for thermal effects induced by 30 keV Ar^+ in $CuInSe_2$ predict that temperatures in the volume of a collision cascade can reach 1700 K during 10^{-11} s.[22]

We speculate that Ar-implantation can form small bubbles, stacking faults, and dislocation loops. In $CuInSe_2$ single crystals, ion implanted with xenon bubbles have been observed by scanning electron microscopy.[23] Transmission electron microscopy studies of $CuInSe_2$ crystals implanted with Xe^+ revealed high concentrations of stacking faults[24] and dislocation loops.[25]

According to TRIM calculations each 30 keV Ar ion creates 525 vacancies and interstitial atoms. Without healing, these defects should amorphize the layer between 6 and 24 nm from the surface after a dose of 10^{15} cm^{-2}. But the first sign of damage is observed in the aligned spectrum after 1.5×10^{15} cm^{-2}. This can be taken to be evidence of the presence of effective healing processes in $CuInSe_2$ at room temperature. After 3×10^{15} cm^{-2}, the total damage is calculated to be 3×10^{16} cm^{-2}, suggesting that only 10 out of 525 created defects per implanted Ar ion were left unhealed. At first sight, it seems remarkable that 98% of the damage can be self annealed at room temperature. But a more accurate consideration of this effect gives even more interesting results. At this dose, only about 10% were calculated to be in the P1 peak, which is related to preferential sputtering, and the rest were found in the P2 peak, which is deeper than the TRIM predicted depth for nonhealed defects and can probably be attributed to stacking faults and dislocation loops, suggesting that more than 98% of the primary defects recombined forming extended defects.

A similar model was developed earlier to explain the results of radiation damage, caused by Ar-implantation into $CuInSe_2$ single crystals, employing Raman scattering and RBS-channeling without a detailed consideration of defect depth profiles.[26] It was suggested that damage is being healed during and shortly after the implantation but that the Ar ions, incorporated at high concentrations in the material, can cause breakdown of the lattice structure. Generally speaking, this model is confirmed by the present data. But the real physical picture of the effects of Ar ion implantation is found to be more complex.

The processes of healing of radiation damage in $CuInSe_2$ single crystals have been studied using transmission electron microscopy and electron diffraction *in situ* with bombardment of the samples with 300 keV ions of Xe^+.[27] It was found that at room temperature such a bombardment cannot randomize the lattice whereas at 50 K a randomization can be achieved.

Although at room temperature implantation primary defects, vacancies and interstitial atoms, recombine the resulting structure, after this is not a perfect chalcopyrite lattice. The recombination generates antisite defects. A positron annihilation study of $CuInSe_2$ single crystals, irradiated with 2 MeV electrons, suggested the formation of antisite defects as secondary radiation defects at room temperature.[28] *Ab-initio* calculations for near stoichiometric $CuInSe_2$ suggest copper on indium site Cu_{In} and indium on copper site In_{Cu} as leading candidates for such antisite defects.[19] The chalcopyrite structure requires ordered positions of copper and indium on the cation sublattice. Their randomization results in the sphalerite structure. The sphalerite to chalcopyrite phase transition takes place at a temperature below the melting point; therefore, the cation sublattice in $CuInSe_2$ always has a degree of randomization.[11] The Cu_{In} antisites at concentrations of 3×10^{20} cm^{-3} were reported in nonirradiated $CuInSe_2$.[29] Thus, high concentrations of the Cu_{In} and In_{Cu} antisites are likely to be present after the Ar implantation.

The evolution of the total damage accumulated in each sublattice (Σ_{Cu}, Σ_{In}, and Σ_{Se}) is shown in Fig. 6. The Cu, In, and Se related curves corresponding to the P2 peak are quite similar gradually saturating with dose. The In curve, corresponding to the P1 peak, does not saturate. This can be interpreted by the formation of an In-rich layer on the surface due to preferential sputtering of Se and Cu.

Evolution of the total damage generated by Ar is similar to that reported for Xe implantation, as also shown in Fig. 6.[15] The Xe-related curve is shifted toward lower doses because of higher rates of damage and sputtering of Xe^+ compared to Ar^+.

The characterization of single crystals of $CuInSe_2$, irradiated with 40 keV xenon ions using RBS/C, has previously been reported.[15] The concentration depth profiles of Cu, In, and Se scattering centers, calculated for xenon implanted areas of $CuInSe_2$, demonstrated only one peak related to a layer of defects. It was shown that maximum concentrations in these profiles achieved 100%, implying amorphization of the material in terms of RBS/C. Now this result can be understood. The effect of preferential sputtering of Se atoms by Ar-ions also takes place for Xe-implantation. According to TRIM-simulations of sputtering of $CuInSe_2$ one 40 keV Xe ion sputters: Cu-1.67; In-1.8; and Se-3.6. Peaks P1 and P2, resolved in the depth profiles after Ar-implantation, are merged together for Xe-implanted $CuInSe_2$ because of the smaller mean penetration depth ($R_{Xe} = 16$ nm) and straggling of Xe^+ ($W_{Xe} = 14$ nm). Therefore, the amorphous layer, observed in $CuInSe_2$ after Xe implantation, can be mostly attributed to preferential sputtering of Se atoms.

V. CONCLUSION

Ar-ion implantation of 30 keV into $CuInSe_2$ single crystal creates two layers of damage: (1) on the surface, caused by the preferential sputtering of Se and Cu atoms; and (2) at the layer of implanted Ar, possibly associated with stacking faults and dislocation loops. The damage is estimated to be less than 2% of TRIM-predicted defects, demonstrating the presence of highly efficient mechanisms of healing of primary implantation defects at room temperature.

ACKNOWLEDGMENTS

This work was supported by the Royal Society, RFBR (14-02-00080, 16-29-06410), and Act 211 of the Government of Russia 02.A03.21.0006.

[1]J. L. Shay and J. H. Wernick, *Ternary Chalcopyrite Semiconductors-Growth, Electronic Properties, and Applications* (Pergamon, New York, 1975).
[2]P. Jackson, D. Hariskos, R. Wuerz, O. Kiowski, A. Bauer, T. M. Friedlmeier, and M. Powalla, Phys. Status Solidi R **9**, 28 (2015).
[3]R. M. Burgess, W. S. Chen, W. E. Devaney, D. H. Doyle, N. P. Kim, and B. J. Stanbery, *The 20th IEEE Photovoltaic Specialists Conference*, New York (1988), p. 909.
[4]M. Yamaguchi, J. Appl. Phys. **78**, 1476 (1995).
[5]A. Jasenek and U. Rau, J. Appl. Phys. **90**, 650 (2001).
[6]W. K. Chu, J. W. Mayer, and M. A. Nicolet, *Backscattering Spectrometry* (Academic, New York/San Francisco/London, 1978).

[7]T. Haalboom, T. Gödecke, F. Ernst, M. Ruble, R. Herberholz, and H. W. Schock, *The 11th International Conference Ternary and Multinary Compounds*, Institute of Physics, Salford, UK (1997), p. 249.
[8]M. Yakushev, A. Zegadi, H. Neumann, P. A. Jones, A. E. Hill, R. D. Pilkington, M. A. Slifkin, and R. D. Tomlinson, Cryst. Res. Technol. **29**, 427 (1994).
[9]M. V. Yakushev, I. I. Ogorodnikov, V. A. Volkov, and A. V. Mudryi, J. Vac. Sci. Technol., A **29**, 051201 (2011).
[10]M. V. Yakushev, I. Pettigrew, A. Jack, Y. V. Feofanov, and A. V. Mudryi, Thin Solid Films **511–512**, 135 (2006).
[11]R. D. Tomlinson, Sol. Cells **16**, 17 (1986).
[12]M. V. Yakushev, G. Lippold, A. E. Hill, R. D. Pilkington, and R. D. Tomlinson, J. Mater. Sci.: Mater. Electron. **7**, 155 (1996).
[13]M. V. Yakushev, V. A. Volkov, I. I. Ogorodnikov, and V. U. Ivanov, Nucl. Instrum. Methods Phys. Res., B **299**, 24 (2013).
[14]E. Bogh, Can. J. Phys. **46**, 653 (1968).
[15]M. V. Yakushev, I. S. Tashlykov, R. D. Tomlinson, A. E. Hill, and R. D. Pilkington, *International Symposium on Materials Science Applications of Ion Beam Techniques*, Seeheim, Germany (1996), Vol. 248-2, p. 171.
[16]T. P. Massopust, P. J. Ireland, L. L. Kazmerski, and K. J. Bachmann, J. Vac. Sci. Technol., A **2**, 1123 (1984).
[17]K. Otte, G. Lippold, D. Hirsch, A. Schindler, and F. Bigl, Thin Solid Films **361–362**, 498 (2000).
[18]J. P. Biersack and L. G. Haggmark, Nucl. Instrum. Methods **174**, 257 (1980).
[19]S. B. Zhang, S.-H. Wei, and A. Zunger, Phys. Rev. B **57**, 9642 (1998).
[20]D. Cahen and L. Chernyak, Adv. Mater. **9**, 861 (1997).
[21]V. Nadazdy, M. Yakushev, E. D. Djebbar, A. E. Hill, and R. D. Tomlinson, J. Appl. Phys. **84**, 4322 (1998).
[22]P. Sigmund, Appl. Phys. Lett. **25**, 169 (1974).
[23]A. Zegadi *et al*., Nucl. Instrum. Methods, B **94**, 429 (1994).
[24]C. A. Mullan, C. J. Kiely, M. V. Yakushev, M. Imanieh, R. D. Tomlinson, and A. Rockett, Philos. Mag. A **73**, 1131 (1996).
[25]J. A. Hinks and S. E. Donnelly, Philos. Mag. **91**, 517 (2011).
[26]G. Lippold, M. Yakushev, R. D. Tomlinson, A. E. Hill, and W. A. Grill, Cryst. Res. Technol. **31**, 381 (1996).
[27]S. E. Donnelly, J. A. Hinks, P. D. Edmondson, R. D. Pilkington, M. Yakushev, and R. C. Birtcher, Nucl. Instrum. Methods B **242**, 686 (2006).
[28]A. Polity, R. Krause-Rehberg, T. E. M. Staab, M. J. Pushka, J. Klais, H. J. Moller, and B. K. Meyer, J. Appl. Phys. **83**, 71 (1998).
[29]C. Stephan, S. Schorr, M. Tovar, and H.-W. Schock, Appl. Phys. Lett. **98**, 091906 (2011).